Failure Analysis of a Sucker Rod from an Oil Well Located Offshore Trinidad and Tobago

Frank Byron
The University of Trinidad and Tobago, Point Lisas Industrial Estate, Point Lisas,
Trinidad & Tobago, W.I.
E-mail: fdbyron54_@hotmail.com

Nazim Mohamed
The University of Trinidad and Tobago, Point Lisas Industrial Estate, Point Lisas,
Trinidad & Tobago, W.I.
E-mail: nazim.mohamed@utt.edu.tt

Clément Imbert
The University of the West Indies, Faculty of Engineering, St. Augustine Campus,
Trinidad & Tobago, W.I.
E-mail: clementimbert40@gmail.com

Abstract

Failure analysis was performed on one of several fractured sucker rods that failed at the stress relief length of the pin-shoulder and the thread of the rods during the fit-up alignment and torque assembly of the rod strings and the couplings. Optical microscopy, scanning electron microscopy and microprobe analysis were utilized to characterize the mode(s) of failure and to analyse the fractured surfaces and inclusions. Brittle flat fractured surfaces were observed for more than 80% of the cross section of the rod. Multiple initiation points of failure propagated from the circumference of the rod which contained machine/grinding marks and a multitude of minute cracks. Microstructure close to the surface of the rod showed transverse cracks propagating from inclusions which were analysed to be manganese sulphide. Torsional load applied to the rod during the assembly added to the stress points on the surface. These surface defects then coalesced into one crack front which propagated in a transgranular shear mode of failure. The recommendations included discontinuing the use of the sucker rods and apprising the supplier of the rods of the material and assembly process deficiencies to seek redress.

*Keywords***:** sucker rods, inclusions, transgranular shear mode failure, Trinidad and Tobago, oil industry

Dr Frank Byron *is a Corrosion Engineer/Metallurgist who holds a Ph.D. Degree from the Process Engineering Department of The University of Trinidad and Tobago (UTT). His research interests include Engineering Metallurgy, Principles and Methodologies of Failure Analysis, Corrosion Studies, Corrosion Prevention and Control Management, Mechanical testing, weld assessments, NDT and in-situ testing.*

Dr Nazim Mohamed *is an Associate Professor at The University of Trinidad and Tobago. He holds a B.Sc. in Applied Chemistry from the University of Portsmouth, England and a Ph.D. in Bioorganic Chemistry from McGill University, Canada. His areas of research include Rheology, Corrosion and Organic Chemistry.*

Professor Clément Imbert *is a Professor Emeritus of The University of the West Indies (UWI). He holds a B.Sc. (Mechanical Engineering) (Hons.) from UWI, M.Sc. (Metallurgical Quality Control) from Brunel University, UK and Ph.D. in Mechanical Metallurgy from UWI, conducted in Canada at Concordia and McGill Universities. His main areas of research are in materials technology, manufacturing processes, inspection and engineering education.*

Introduction

Cost effective failure management begins with prevention. Marginal producing wells with high failure frequency rates are often classified as uneconomic and effective failure management practices can mean the difference between economically operating these wells and plugging them (Hendricks & Stevens, 2006). Achievable failure frequency reduction requires accurate root cause analysis and the implementation of corrective measures to prevent recurrence. Sucker rod failures are due to a number of causes including Design Deficiencies. This may involve notches at high stress points and poor material selection which can accelerate fatigue failures. Manufacturing Deficiencies include discontinuities in castings and imperfections in forgings and weldments. Then there are Processing Deficiencies which involve machining and grinding marks, heat treatment and identification markings (Payer, 1994).

Sucker Rods are long-jointed steel rods threaded at both ends and joined, to form a sucker rod string. They are used to connect the downhole components in a well by this string arrangement to the pumping jack at the surface. They transfer the rotary motion energy of the drive unit to the down-hole pump assembly to pump and retrieve fluids. A Sucker Rod can range from 7-9 m (25-30 ft.) in length (Ghen & Liu, 2016).

In recent years, class C and class D (carbon steel) sucker rods have become incapable of meeting the production process requirements for deeper, heavy oil wells. Thus, ultra-high strength sucker rods have been introduced due to their superior strength and other mechanical properties. It has been proved that sucker rod failures are mostly caused by fatigue or corrosion fatigue, so it is important to understand the fatigue problems of the ultra-high strength sucker rods to obtain a reliable fatigue life prediction model (Li et al., 2015; Liang et al., 2017; Niu et al., 2018). Premature fatigue failure can lead to problems including a reduction in oil recovery rate and production, as well as an increase in operational cost. It is therefore necessary to use heat treatment processes on these improved alloy steel sucker rods to mitigate fatigue failures (Dong et al., 2021; Zhao, 2021).

Several researchers have examined the fatigue life of ultra-high strength sucker rods. For example, Lin Yuanhua et al. used the Forman model to predict the fatigue life of a sucker rod with or without initial cracks (Lin et al., 2005). Fan Song et al. (2017) assumed that sucker rod fatigue data obeyed normal distribution and derived a fatigue life prediction model by fitting the Basquin formula in the form of a power function. Li Qi et al. (2006) used the static characteristics of sucker rods to predict fatigue performance and proposed a fatigue life prediction method considering the cumulative damage factors. Song Kaili et al. (2003) processed sucker rod fatigue data with log-normal distribution and obtained the maximum stress versus fatigue life (S-N) curve in linear form.

Most of the existing fatigue models for sucker rods are based on the Basquin linear model, which assumes that the S-N (Stress-Number of Cycles) data obeys normal distribution. Using the least squares method to estimate the value of the parameters, the relationship between stress and high cycle fatigue life can be obtained, which is used to determine the P-S-N curve (where P is the reliability) (Least Square Method - Definition, Graph and Formula). However, the Basquin model has some limitations. It is well known that the Weibull distribution is the most suitable distribution for survival and life analysis. Since it can easily calculate the distribution parameters by probability value, it is widely used in the processing of experimental data related to fatigue life (Cheng et al., 2019; Park et al., 2016; Strzelecki, 2021).

Several recently purchased sucker rods, for assembly of an oil well located offshore Trinidad and Tobago's coast, failed prematurely during the fit-up alignment and torque assembly of the rod string with the couplings. The fractures occurred within the stress relief lengths of the pin shoulders and the threads of the rods. The objective of the study is to introduce the forms of material degradation that occur during the service life of components which do not satisfy design conditions; it also illustrates specific features of attack that alert operators and inspectors about potential failures. Failure analysis was then performed to determine the root cause of failures and to recommend procedures to prevent reoccurrences.

Approach

The analysis undertaken of the failed sucker rods comprised the following:

1. Visual Inspection. The failed sucker rod samples were visually inspected and digital photographs were taken.
2. Dimensional Measurements. Dimensional measurements of the failed sucker rod samples were taken using a Digital Calliper.
3. Macrography. A macroscope, with digital imaging capability, was used to observe the samples at macro level and to photograph features of interest.
4. Metallographic Analysis. An Optical Microscope was used in the analysis, and photomicrographs were taken at points of interest.

5. Micro-fractography and Microprobe Analysis. A Scanning Electron Microscope (SEM), with an attached Energy Dispersive Spectrometer (EDS), was used to record areas of interest.
6. Hardness Testing. A Vickers Hardness Tester was used to determine macro and micro hardness profiles. Testing was carried out using guidelines given in ASTM E384 "Standard Test Method for Knoop and Vickers Hardness of Materials" (Weatherford, 2015). A hardness scale HV 10 was selected.
7. Elemental Analysis. The analysis was carried out using an Optical Emission Spectrometer (OES). The carbon and sulphur contents were determined using a Carbon/Sulphur Determinator.

Results

Visual Inspection

The visual inspection of sucker rods revealed that the fractures occurred closer to the shoulder of the stress relief region between the pin shoulder and the threads of the rods. The stamped letters on the wrench square section indicated the type of rod. There were no markings indicating the rods' specifications and year of manufacture. The typical fracture position is shown (Figure 1). The fractured cross-section was relatively flat with a brittle mode of failure for more than 80% of the rod and ductile section that indicated final fracture zones. There were also severe abrasions in the ductile regions. A typical fracture is shown (Figure 2).

Figure 1

Fracture at Shoulder (red arrow). Note wrench square section (blue arrow).

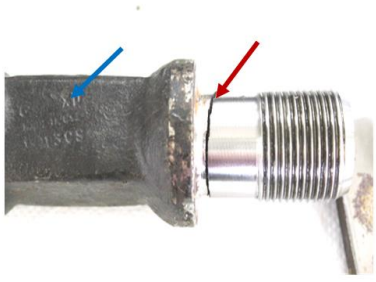

Figure 2

The fractured cross-section is flat and brittle (red arrows); fast fracture severe abrasion (yellow arrow).

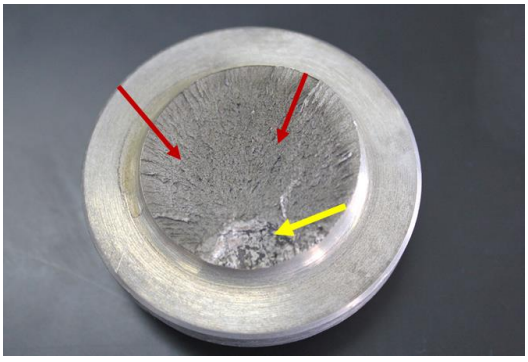

Dimensional Measurements

Average dimensional measurements of the sucker rods were recorded. The measurements were compared with the general diameter and tolerances for steel sucker rods given in API specification 11B (American Petroleum Institute API SPEC 11B, 2010). The results are presented in Table 1.

Table 1

Dimensional Measurements

Sucker Rod Dimensional Position	Measurements (mm)	*API 11B Specification Tolerances (mm)*
Diameter of rod body	28.38	*28.07-28.83*
Diameter of rod Bead	51.83	*49.25-55.73*
Diameter of Stress Relief section	35.93	*35.79-36.05*
Diameter of pin shoulder (Outside)	57.09	*56.82-57.58*
Width of wrench square section	37.72	*37.30-38.90*
Length of wrench square section	42.64	*41.3 min*
Length of stress relief section	22.23	*22.23-23.02*

Dimensions satisfied the requirements of API 11B 'Specification for Sucker Rods'.

Macro-fractography

Macro analysis of the sample revealed that the fractured surface showed multiple crack propagation sites (Figure 3). The surface of the rod also showed machine/grinding marks and a multitude of minute cracks emanating and propagating along these processing marks close to the fractured regions (Figure 4).

Figure 3

Multiple crack propagation sites on the circumference of the rod (red arrows).

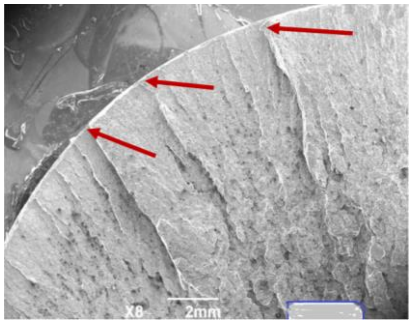

Figure 4

Minute cracks emanating close to the fracture region (red arrows).

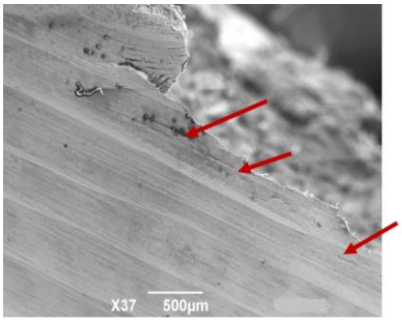

Metallographic Analysis

Sections of the sucker rods were ground, polished and etched, and microstructure revealed a fine-grained normalized and tempered structure. Also of note was the high inclusion level in the matrix (Figure 5). Longitudinal sections close to the main fracture showed transverse cracks propagated perpendicular through the axis of the rods in transgranular modes. The feature is seen in Figure 6.

Figure 5
A typical microstructure. Note high inclusion content (red arrows)

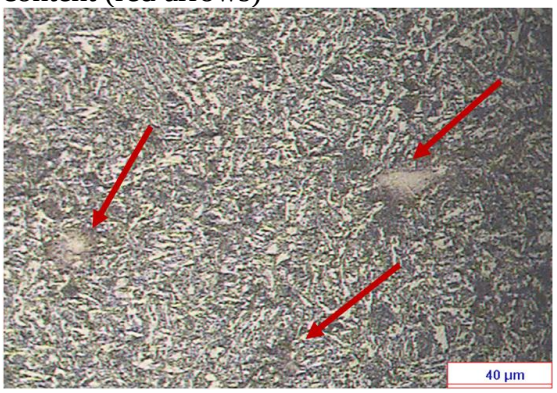

Figure 6
A transverse crack propagating (red arrows).

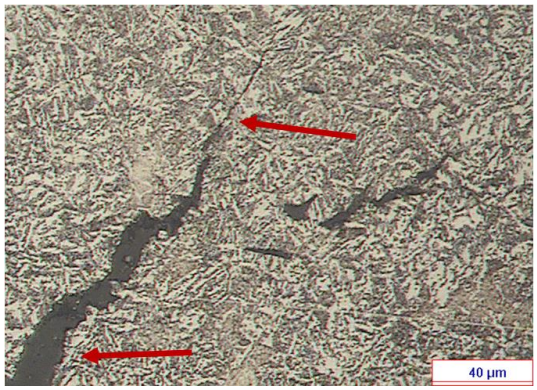

SEM analysis of longitudinal sections close to the fractured regions showed typical features of a transverse crack propagated from an inclusion at the surface of the rod (Figure 7). There were inclusions in the matrix that were greater than 200 µm in width (Figure 8). Secondary cracks propagated along the lines of the stringer inclusions. Also of note was cracking at the inclusion interface and spaces where inclusions were once lodged (Figure 9).

Figure 7
A transverse crack propagated from an inclusion at the surface (red arrow).

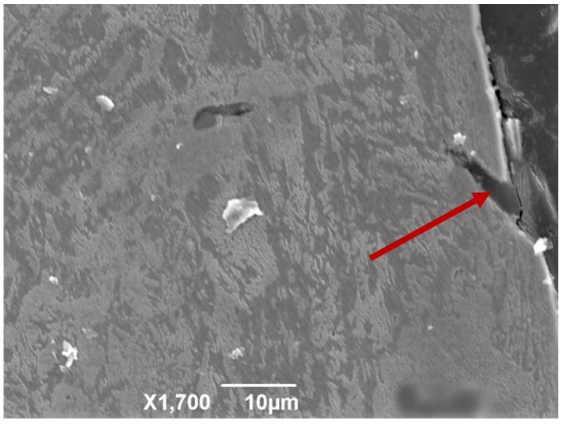

Figure 8
Inclusions greater in width than 200 µm (red arrows).

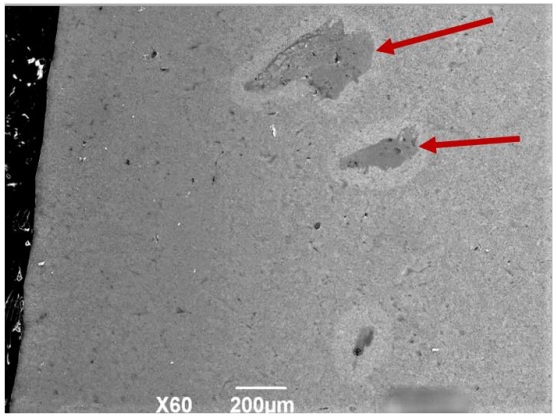

Figure 9
Cracks Propagating along the Lines of the Stringer Inclusions (red arrows).
Also note inclusions have fallen out of the matrix (blue arrows).

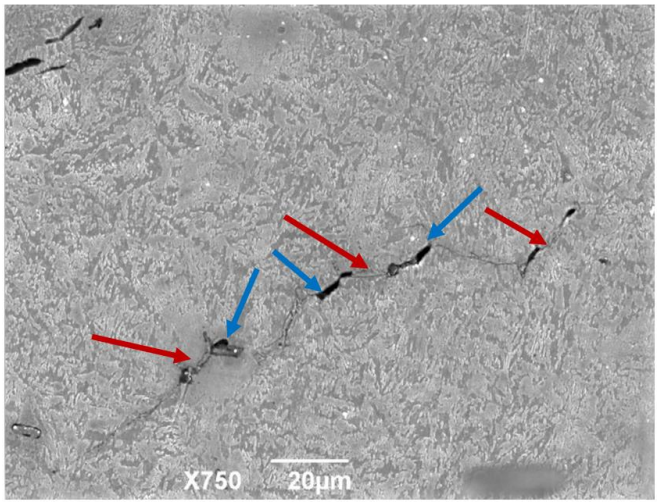

Micro-fractography and Microprobe Analysis

A fractograph of the rod revealed multiple cracks propagated from machine/grinding marks at the surface (Figure 10). Figure 11 is a fractograph showing a brittle transgranular shear mode of failure. The final fracture zone showed ductile micro-void coalescence within the mechanically damaged (abraded) region (Figure 12). Multiple crack openings at inclusions and machine/grinding marks on the circumference of the rod adjacent to the main crack are shown in Figure 13.

Figure 10
Multiple Cracks Propagating from Machine/grinding Marks (red arrows).

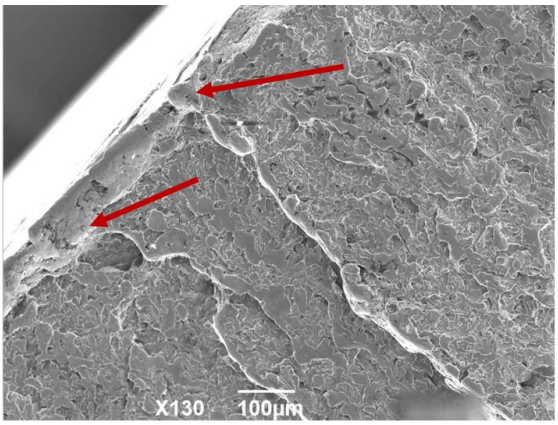

Figure 11
A Brittle Transgranular Shear Mode of Failure (red arrows)

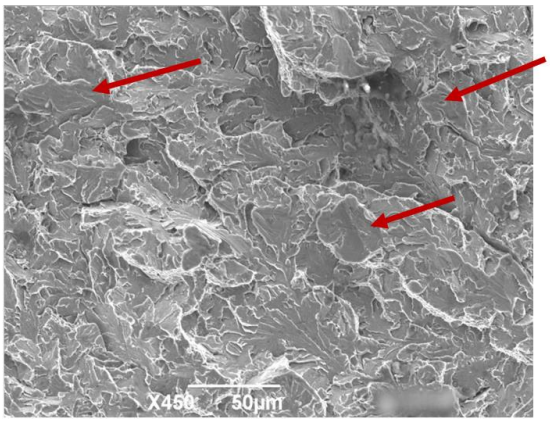

Figure 12
Micro-void coalescence (red arrows) within abraded region (blue arrows).

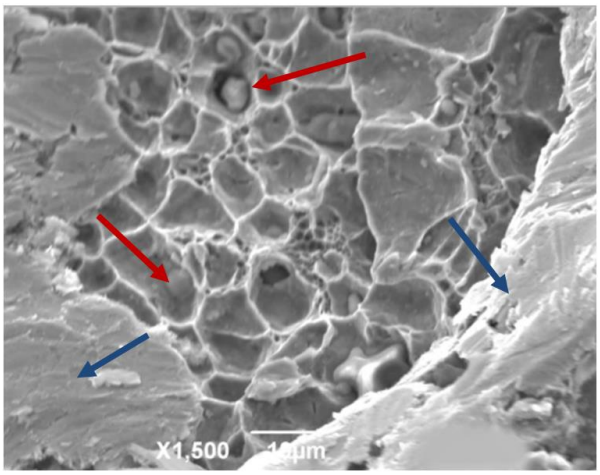

Figure 13
Multiple crack openings at inclusions and machine marks (red arrows).

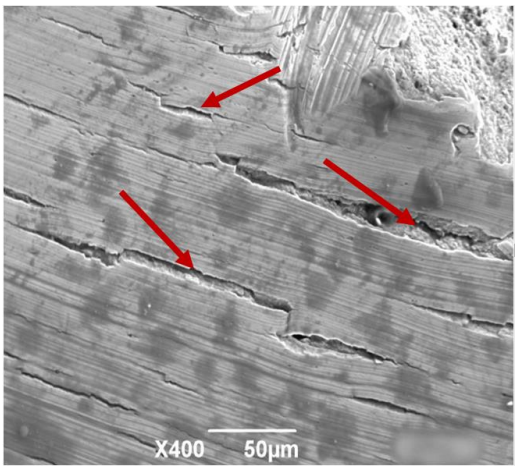

Microprobe analysis of samples revealed stringer-like inclusions that were analysed to be manganese sulphide. Also of note was cracking at the inclusions and the voids that followed (Figure 14). Circular shaped inclusions were also analysed to be manganese sulphide with a trace of oxygen (Figure 15).

Figure 14

Stringer like inclusion showed the compound manganese sulphide and also showed cracking and a void.

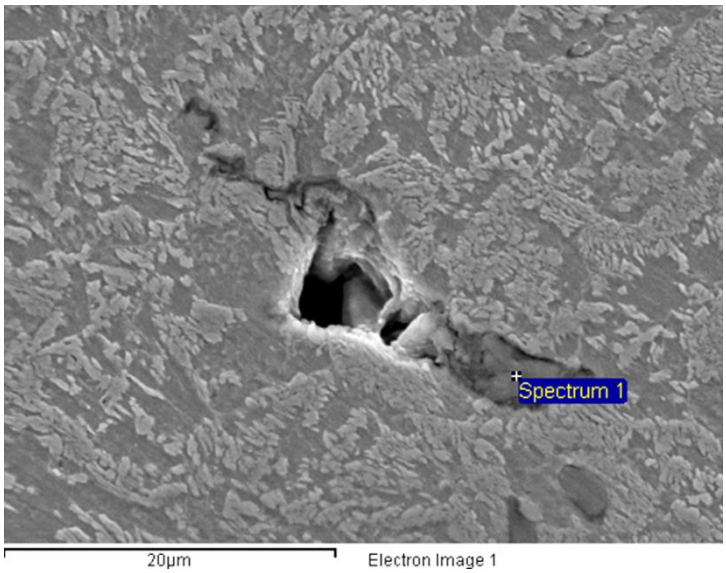

Element	Weight %
Si	0.44
S	33.95
Mn	52.04
Fe	13.57
Totals	100.00

Elemental analysis of stringer inclusion in Spectrum 1

Figure 15

Elliptical shaped inclusion showed (a) that was identified as manganese sulphide.

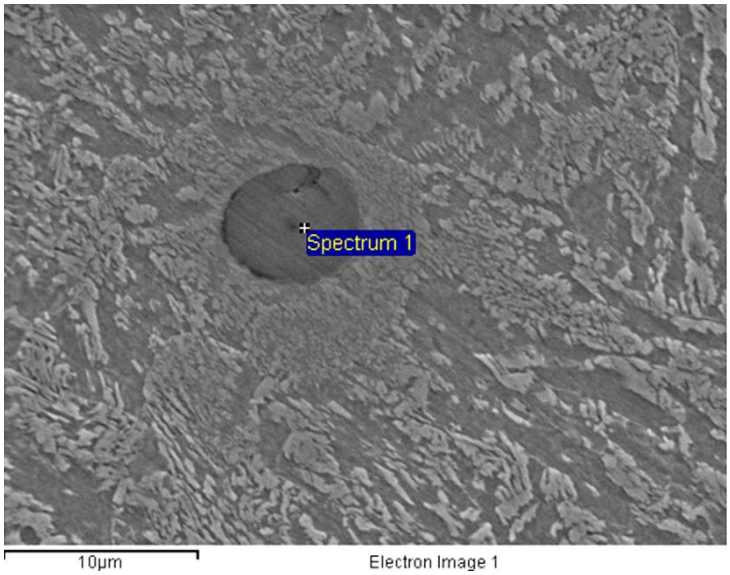

Element	Weight %
S	37.64
O	6.15
Mn	52.55
Fe	3.66
Totals	100.00

Elemental analysis of elliptical inclusion in Spectrum 1

Vickers Hardness Test (HV10)

Vickers (HV10) hardness profile measurements were taken on a cross-section of polished samples. The values were taken approximately 1 mm apart from each other from the outer radius of the rod to the inner core. The hardness readings are presented in Table 2.

Table 2
Vickers Hardness Test (HV10)

Test No. (1 mm apart)	*1*	*2*	*3*	*4*	*5*	*6*	*7*	*8*	*9*	*10*
Hardness Values HV (10)	304	307	301	305	305	302	292	309	290	305

The results indicate a consistent hardness throughout the micro structures within allowable tolerances.

Elemental Analysis
Quantitative elemental analysis of the samples was compared with API grade 4138 M Chromium-Molybdenum alloy steel as shown in the Sucker Rod specification (American Petroleum Institute API SPEC 11B, 2010). The results are presented in Table 3.

Table 3
Quantitative Elemental Analysis of Sucker Rod

Elements	***Percentage composition by weight %***	
	Rod	***API grade 4138 M***
Carbon	0.410	*0.380 - 0.420*
Sulphur	0.040	*0.040(max)*
Phosphorus	0.015	*0.035(max)*
Manganese	1.29	*1.00 – 1.30*
Silicon	0.25	*0.20 – 0.35*
Chromium	0.59	*0.55 – 0.85*
Molybdenum	0.26	*0.24 – 0.32*
Nickel	0.08	*0.30 (max)*
Vanadium	0.09	*0.08-0.11*
Copper	0.26	*0.35 (max)*
Iron	Remainder	Remainder

The sample satisfied the chemical requirements of API grade 4138M chromium-molybdenum alloy steel as shown in the Sucker Rod specification.

Discussion

Visual examination of the failed sucker rods from an oil-well offshore Trinidad and Tobago showed that the fracture occurred closer to the shoulder of the stress relief region between the pin shoulder and the threads of the rod (Figure 1). Further examination showed that failure emanated from surface features on the rod (Figures 4 & 7). These features created multiple initiation sites for cracks to nucleate, propagate and coalesce to form one crack front showing a brittle transgranular shear mode of failure for more than 80% of the diameter of the rod (Figures 2, 3, 10 & 11) and then parted to depict a tensile overload ductile mode of failure. The ductile region subsequently experienced mechanical damage in the form of abrasion marks post failure. Small sections of micro-void coalescence were observed on the fractured surface in areas of the ductile region (Figure 12).

The Vickers profile hardness results of the sample following the guidelines given in ASTM E 384-17 "Standard Test Method for Knoop and Vickers Hardness of Materials" showed a consistent hardness throughout the material (ASTM E 384-17, 2017). The Elemental analysis showed that the rod satisfied the API 4138M chromium–molybdenum alloy steel chemical composition (Table 3).

Metallographic analysis of the rod showed a normalized and tempered microstructure~~,~~ that contained a number of inclusions having different sizes and shapes and randomly oriented throughout the matrix (Figures 5, 7, 8 & 9) including the surface and subsurface. The inclusions were identified as sulphides and oxides, with the majority being manganese sulphide compounds (Figures 14 & 15). It should be noted that the shape of the inclusions plays an important part in determining whether notches can be created to encourage stress points for fatigue to initiate. Cracks were observed propagating from the irregular-shaped inclusions that "emanated" to the surface of the rod and propagated along the machine/grinding marks that were also observed on the surface of the rod (Figures 4, 7, 10 & 13). The cracks then propagated through the axis of the rod along lines of least resistance, that is, the irregular-shaped inclusion sites within the matrix of the steel (Figures 6 & 9).

The composition, size, number and distribution of inclusions determine the cleanliness of steel, and this can be classified and rated by severity levels following the ASTM E 45-18a Standard Method "for Determining the Inclusion Content in Steel" (ASTM E 45-18a, 2018). The inclusions can be classified as class 'A' heavy inclusion and can fall in a high severity rating following the ASTM E 45-18a Standard. Large irregular-shaped inclusions are responsible for notch sensitivity, creep and poor fatigue properties of the steel. These non-metallic inclusions are derived from the steel-making process. Inclusions may not be evenly distributed within the steel, and, therefore, it is possible that different properties of the steel may be obtained at varying positions from the same

steel ingot or slab. Inclusions with irregular shapes and sharp edges (as observed in the sucker rod), when compared to inclusions with a smooth rounded shape, cause larger stress concentration points, and this makes it easier for a fatigue crack to initiate (Juvonen, 2004).

Fatigue cracks may also initiate through the inclusion cracks, or they may initiate from the interface between the different phases of the inclusion (Figure 14). Fatigue crack initiation is dependent on the stress concentration factor of the defect. Differences in the thermal expansion coefficients of the inclusion and the matrix can generate internal stresses around inclusions (Niclas et al., 2015). During the hot working of the steel, the stresses between inclusions and the steel matrix are relaxed, but when cooling occurs, tensile residual stresses are generated around the inclusions which causes problems.

Sulphide inclusions give rise to voids at the interface between the inclusions and matrix, and these stresses greatly alter the properties of the matrix and may cause microcracks at the metal/inclusion interface (Niclas et al., 2015). Microcracks already present in the metal at the beginning of service may then be the origin of later fatigue fracture. Nonmetallic inclusions at or close to the surface are detrimental because they form points for initiation of fatigue cracks (Figure 7); the larger the number of discontinuities, the greater the possibility of fatigue failure. The machine/grinding marks also create the notch effect and stress raisers similar to the behaviour of inclusions.

Conclusions

The failure occurred due to material and processing deficiencies. There were manganese sulphide inclusions, many of which were irregularly shaped and randomly dispersed throughout the matrix of the structure, especially those that were at or close to the surface of the rods. Stress concentration points due to these inclusions and machine/grinding marks were created at the interface of the rod's shoulder and the stress relief region. Torsional load applied to the rods during the assembly added to the stress points and created notch effects where the local stress exceeded the material proportional limit and opened up the microcracks that were already at the inclusion interfaces.

The cracks propagated along the stress points on the surface of the rods. The cracks then propagated inwards along the lines of the inclusion sites and then formed one crack front. The sucker rods then fractured in two leaving a failure mode that included a brittle transgranular shear mode zone and a final ductile tensile overload region as observed on the fractured surface.

Recommendations

Sucker rod failure prevention begins with proper design, materials, processing and finishing operations. The material must satisfy certain conditions in terms of strength, toughness and morphology including inclusion content as well as proper identification markings. Processing and finishing operations should not introduce defects including stress raisers. For example, machine/grinding marks should not be present on the surface of the rod as they create stress points for cracks to initiate (American Petroleum Institute API SPEC 11BR, 1989). It is recommended that the use of the defective batch of sucker rods be discontinued, and the supplier be apprised of the material and processing deficiencies.

References

American Petroleum Institute API SPEC 11BR. (1989). *Recommended practice for care and handling of sucker rods* (8th ed.).

American Petroleum Institute API SPEC 11B. (2010). *Specification for sucker rods, polished rods and liners, couplings, sinker bars, polished rod clamps, stuffing boxes, and pumping tees* (27th ed.).

Anmark, N., Karasev, A., & Jonsson, P. G. (2015). *The effect of different non-metallic inclusions on the machinability of steels.* Department of Materials Science and Engineering Royal Institute of Technology; Stockholm Sweden.

ASTM E 384-17. (2017). *Standard test method for micro-indentation hardness of materials.* ASTM International, West Conshohocken, PA.

ASTM E 45-18a. (2018). *Standard test method for determining the inclusion content of steel.* ASTM International, West Conshohocken, PA.

Cheng, X., Huang, G., Wei, T., Meng, F., & Zhao, L. (2019). *Test method of P-S-N curve of cylinder head material and selection method of fatigue model*. Veh. Engine.

Dong, Z., Tong, Z., Zhou, H.-Y., Wang, H.-M., Zheng, W.-Y., Sun, X.-R., & Ding, H. (2021). *Development of steel for sucker rod and failure of sucker rod in service*. Mater. Rev.

Fan, S., Liang, Y., Wang, L., Lei, Y., & Shi, H. (2017). *Calculation of allowable stress and fatigue life prediction method for H-class sucker rod*. Pet. Drill. Tech.

Ghen, G. S., & Liu, X. (2016). *Friction dynamics of oil-well drill strings and sucker rods*. Science Direct Elsevier Ltd.

Hendricks, C. T., & Stevens, R. D. (2006). *Sucker rod failure analysis: A special report from Alberta Oil Tool*. T6E 0C1 Edmonton Alberta.

Juvonen, P. (2004). *Effects of non-metallic inclusions on fatigue properties of Calcium treated Steels.* Department of Mechanical Engineering; Helsinki University of Technology.

Least Square Method - Definition, Graph and Formula). https://byjus.com /maths/least-square-method/

Li, D., Lu, M., Guo, J., Zhang, J., Liu, T., & Liang, Y. (2015). *Experimental analysis of fatigue performance of H-class sucker rod*. Oil Field Equip.

Li, Q., Liu, D., & Li, X. (2006). *Determination of service period of in-service sucker rod. J. Northeast.* For. Univ. 2006, 34, 111–112+114.

Liang, Y., Zhao, C., Zhong, Y., Fan, S., Shi, H., & Lei, Y. (2017). *Fatigue performance analysis of super high strength sucker rod*. Drill. Prod. Eng.

Lin, Y., Zhang, D., Luo, F., Shi, T. (2005). *Research on fatigue life calculation of sucker rod*. Pet. Drill. Prod. Technol.

Niu, C., Cui, W., Zhu, H., Wang, B., Shi, H., & Liang, Y. (2018). *New design method and application of H-class sucker rod*. Oil Field Equip.

Park, J. P., Chanseok, P., Jongweon, C., Chi, B. B., & Jordi, F. (2016). *Effects of Cracking Test Conditions on Estimation Uncertainty for Weibull Parameters Considering Time-Dependent Censoring Interval*. Materials.

Payer, J. H. (1994). *Sources of failure*. Department of Materials Science and Engineering: Materials Engineering Institute USA.

Song, C. (2003). Experimental study on P-S-N curve of super-high strength sucker rod. *Oil Field Equip, 32*, 27–29.

Strzelecki, P. (2021). *Determination of fatigue life for low probability of failure for different stress levels using 3-parameter Weibull distribution.* Int. J. Fatigue.

Weatherford. (2015). *High strength sucker rods special chrome-moly alloy steel, normalized; tempered and induction Case Hardened.* https://www. weatherford.com /en/ documents/brochure/products-and-services/production-optimization/sucker-rods/

Anmark, A. (2015). The effect of non-metallic inclusions of steel welds. https://ewi.org/the-effect-of-non-metallic-inclusions-in-the-cghaz-of-hsla-steel-welds/

Zhao, Z. (2021). *Reasons and prevention measures of sucker rod break in oil well*. Chem. Eng. Equip.